International Journal of Applied Mathematics

Volume 38 No. 3s, 2025

ISSN: 1311-1728 (printed version); ISSN: 1314-8060 (on-line version)

ENHANCED BRAIN TUMOR SEGMENTATION AND CLASSIFICATION USING CAPSULE NETWORK AND EFFICIENTNETB3

[*1a,b] Sandhya Sandeep Waghere, [2] Dr. Mahip M Bartere, [3]Dr. Shrikant Chavate

[*1a)] Research Scholar, Department of CSE,

G H Raisoni University, Amravati, Anjangaon, Maharashtra, 444701-India.

[*1b)] Assistant Professor, IT Department,

Pimpri Chinchwad College of Engineering, Pune, 411044, India

[2]Associate Professor, Department of CSE,

G H Raisoni University, Amravati, Anjangaon, Maharashtra, 444701-India.

[*]Corresponds Email: wagheresandhya82@gmail.com

*Email: mahip.bartere@gmail.com

[3]Associate Professor

Dept of Electronics and Telecommunication Engineering

G H RAISONI UNIVERSITY AMRAVATI

shrikant.chavate@ghrua.edu.in

spchavate@gmail.com

Abstract

Brain tumors pose a significant threat to both young and older individuals. Despite advancements in machine learning (ML) and deep learning (DL) techniques for brain tumor segmentation and detection, challenges persist, including low performance, high computational complexity, and insufficient data. This study proposes an efficient multi-modal brain tumor segmentation and classification method using a combination of Capsule Network and EfficientNetB3. Initially, T1, T2, and Flair MRI images are pre-processed using Upgraded Mean Filtering (Up-MFil), image resizing, and HSV color channel conversion. Segmentation is then performed using Gannet-based Kapur's Thresholding (GKT), followed by feature extraction and optimal feature selection using the Gannet Optimal EfficientNetB3 model. Finally, the brain tumors are classified into High Grade Glioma (HGG) and Low Grade Glioma (LGG) using the Fine-Tuned Hybrid Deep Convolutional Capsule Network (FT-HDC^{2}Net). The proposed technique is evaluated on the BraTS 2018 dataset, achieving 98% accuracy, 96.52% precision, and 94.03% recall. Compared to other related techniques, the proposed

Received: July 18, 2025

International Journal of Applied Mathematics

Volume 38 No. 3s, 2025

ISSN: 1311-1728 (printed version); ISSN: 1314-8060 (on-line version)

method demonstrates superior performance in terms of accuracy, precision, recall, F1-score, specificity, and Kappa. Additionally, the method achieves low error rates and fast computational times, highlighting its potential for efficient brain tumor segmentation and detection.

Keywords: MRI image, Mean Filtering, Kapur's Threshold, EfficientNetB3, Capsule Network, HGG, LGG, Gannet Optimization.

1. Introduction

Brain tumors are a most dangerous disease that arises from abnormal cell growth in the brain or spreads to the brain cells. When a tumor causes pressure on healthy brain regions and spreads to those areas, it is more damaging. This stage would eventually lead to cancer [1]. While not all brain tumors are cancerous, all brain malignancies are tumors. Benign brain tumors are non-cancerous brain tumors. Brain tumors are categorized into four major types: Grade I and II brain tumors, which are known as benign (non-cancerous), and Grade III and Grade IV, which are known as malignant tumors (cancerous) [2]. Grade I and II tumors are referred to as LGG, and grade III and IV tumors are referred to as HGG. In India, around 30,000 people are affected by a brain tumor every year, which is reported by the Indian Council of Medical Research (ICMR) [3, 4]. There are nearly 120 types of brain tumors, categorized based on their location, type of tumorcells, and complexity. More than 80% of all Central Nervous System (CNS) malignancies are brain tumors [5].

Brain tumors are categorized into two major types: primary and metastatic. Primary brain tumors occur when abnormal or malignant cells develop within brain cells, such as meningioma (35%), pituitary (14%), and glioblastoma (16%) [6]. A benign tumor known as a meningioma develops from the membranes that surround the brain and spinal cord. Pituitary tumors are benign tumors that develop from aberrant growths in the pituitary gland [7-8]. The metastatic tumor develops when cancer cells move from another damaged body part into the brain. Medical imaging employs a variety of imaging techniques, such as computed tomography (CT) scans, X-rays, Positron Emission Tomography (PET)/Magnetic Resonance Imaging (MRI) scans, magnetic resonance spectroscopy (MRS), functional magnetic resonance imaging (fMRI), and so on [9].

Although structural MRI scans give information regarding brain tumors on a cellular, functional, metabolic, as well as vascular level [10], radiologists support these scans for brain tumor diagnosis. Multi-orientation and multi-modality MRI can provide a reliable diagnosis of brain tumor tissue. The multi-modal MRI includes T1, T1-Gadolinium (T1-Gd), T1-Weighted (T1-W), T2, T2-W, Fluid Attenuated Inversion Recovery (FLAIR), and additional modalities [11, 12]. The various tumor tissues such as edoema, necrosis, enhancing, and non-enhancing tissues are examined with these modalities. Active tumors can be detected with T1Gd, the tumor core can be identified with T2, and the entire tumor can be identified with the T2 FLAIR modality [13]. T2-W MRI signifies that the edoema tissue around the tumor is shining, as seen in the MRI image. Furthermore, axial, coronal, and sagittal orientations of MRI are presented

Received: July 18, 2025

Volume 38 No. 3s, 2025
ISSN: 1311-1728 (printed version); ISSN: 1314-8060 (on-line version)

in the MRI images [14]. The various modalities offer different biological data that may be evaluated using basic quantitative metrics for disease progression, treatment planning, and tumour diagnosis in clinical routine [15].

Several techniques, including machine learning (ML) as well as deep learning (DL), are used to segment and classify brain tumors [16]. The hand-crafted features are widely used for automatic brain tumor segmentation, with features generated for classifiers using standard ML models. Support vector machines (SVMs) are commonly utilized approaches for brain tumor segmentation [17, 18]. These techniques could fail to detect the general structure of the target objects or extract high-level features due to the focus on minute details, such as image textures. Convolutional neural network (CNN) is a DL-based technology. Some CNN-related techniques, such as 3-dimensional CNN and Deep CNN, have been adopted for classification purposes. The FSENet is a binary classification technique aimed at providing better recognition of a brain tumor's sub-structure [19, 20].

Several techniques were also analyzed for feature extraction and classification purposes from various domains. Multimodal Knowledge Extraction and Accumulation on Hyperplanes (MKEAH) was developed to ensure the lengths of feature vectors on hyperplanes [21]. An importance-aware 3D volume visualization method was developed to retrieve images from large imaging repositories, which optimized the rendering parameter automatically to improve the clear structure visibility [22]. 3D Slicer software was developed by integrating the genuine scene virtually to establish 3D brain tumor reconstruction [23]. A multi-scale spatio-temporal attention network (MSSTANet) was developed by integrating the convolutional residual squeeze and excitation (CRSE) module with multi-branch convolution and long short-term memory (MCLSTM) model to improve the accuracy of user action recognition [24]. An Embedded Clustering Sliced U-Net (ECSU-Net) was developed to perform segmentation, intervertebral disc extraction (IDE), and fusion [25]. An Optimally Fused Fully end-to-end Network (OFF-eNET) was developed for automatic segmentation of the volumetric 3D intracranial vascular structures [26]. Optical-flow based large-scale slice augmentation named (SOFNet) was developed by using the optimal-flow based and encoder-decoder backbone to interpolate MRI slices while preserving feature consistency [27].

1.1 Motivation

Larger datasets are required to assess the efficiency of various techniques for diagnosing brain tumors. A few models have increased computational complexity, which reduces the overall efficacy of brain tumor identification. A few brain tumor classification algorithms were developed to reduce overfitting in the dataset; however, they generated an enormous quantity of noise during training. During the process of segmenting the MRI image, some significant limitations included time complexity, high processing costs, and the necessity for additional parameters. Several treatments are less effective when the dimensions, as well as the position of brain tumors, are not accurately identified. Brain tumors frequently exhibit inhomogeneous intensities in their MRI images, which are limited by imaging principles. The MRI image reveals overlapping and unclear borders between the tumor and the surrounding tissues. To

Received: July 18, 2025

Volume 38 No. 3s, 2025
ISSN: 1311-1728 (printed version); ISSN: 1314-8060 (on-line version)

overcome this kind of issue, the proposed technique is developed to provide efficient brain tumor segmentation and classification. The main contribution of the suggested method is discussed below.

- To enhance the image quality, efficient pre-processing techniques such as Upgraded Mean Filtering (UP-MFil), image resizing, and HSV color channel conversion are used.
- To segment the pre-processed image, Gannet-based Kapur's Thresholding (GKT) scheme is used based on WT, TC, and ET.
- To extract the optimal features, the Gannet Optimal EfficientNetB3 (GO_ENetB3) model is used, and it also reduces dimensionality issues.
- To classify the tumor as HGG and LGG, the Fine-Tuned Hybrid Deep Convolutional Capsule Network (FT-HDC^{2}Net) model is utilized.

The remaining content of the paper is organized in the following manner: Section 2 includes the survey of some related techniques over multi-modal brain tumor segmentation and classification. Then, the techniques utilized in the proposed methodology are described briefly in Section 3, with Figures. The Results obtained by the proposed method are analyzed and discussed in Section 4. Finally, the overall conclusion of the paper is shown in Section 5.

2. Related Works

A survey of some related techniques over brain tumor segmentation and classification is described briefly.

M.O. Khairandish et al. [28] developed a hybrid model that combined CNN and SVM to classify the brain tumor. The Maximally stable external regions (MSER) technique is utilized to pre-process the image. The segmentation is performed with threshold-based segmentation techniques. This model achieves 98.49% accuracy, and limited features are considered for feature extraction. The BRATS 2015 dataset used in this model is obtained from BRATS 2012 and BRATS 2013.

Ilyasse Aboussaleh et al. [29] developed a CNN-based technique for predicting as well as segmenting brain tumors. A simple binary annotation is utilized to reflect the existence of the tumor or not. This model utilized the BraTS 2017 dataset with various kinds of gliomas. It achieves 91% accuracy in tumor classification and 82.35% Dice similarity coefficient for tumor segmentation. This technique is only utilized to test FLAIR modalities of RMR images in the dataset.

Nagwan Abdel Samee et al. [30] developed a lightweight, effective U-Net deep network to perform real-time segmentation. Simplified deep CNN (DCNN) was used to assess as well as classify brain tumor features automatically. This model utilizes the BRATS 2015 dataset for brain tumor classification. This model achieves 88.6% accuracy, 88.8% Dice similarity coefficient (DSC), and 89.4% sensitivity by classifying the HGG and LGG tumors.

R. Pitchai et al. [31] used a combination of Artificial Neural Network (ANN) as well as Fuzzy K-means algorithms to segment tumor locations. This model comprises four stages: noise

Received: July 18, 2025

Volume 38 No. 3s, 2025
ISSN: 1311-1728 (printed version); ISSN: 1314-8060 (on-line version)

removal, attribute extraction and selection, classification, as well as segmentation. Wiener filters are used to eliminate noise, GLCM is used to extract features from images, and the Crow Search Optimization method is used for feature selection. The DL-based classification is used to distinguish between aberrant as well as normal images. Finally, the Fuzzy K-Means algorithm is utilized for segmentation. This model utilized the BRATS dataset, achieving 94% accuracy.

Angona Biswas and Md. Saiful Islam [32] developed a three-class brain tumor classifier. Initially, the images were pre-processed using a sharpening filter, resizing as well as contrast development. A K-means clustering algorithm is utilized to pre-process data, as well as a 2-dimensional discrete wavelet transform is utilized for feature extraction. The feature quantity reduction method relied on principal component analysis. At last, Artificial Neural Network (ANN) is used to identify brain tumors such as glioma, meningioma, or pituitary-type tumors. This model achieves 95.4% accuracy, and high computation complexity occurred while performing the classification.

The new lightweight segmentation model MicrowaveSegNet (MSegNet) was utilized to segment the tumor region in light of the time consumption of current brain tumor detection methods. Reconstructed microwave (RMW) brain pictures were classified using a classifier called the BrainImageNet (BINet) model. These methods were created by Amran Hossain et al. [33] to enhance the segmentation and classification of brain tumors. The accuracy and Dice Score of this method for classifying and segmenting brain tumors are 89.33% and 93.10%.

R. Poonguzhali et al. [34] developed an Automated Deep Residual U-Net Segmentation with a Classification model (ADRU-SCM) for brain tumor diagnosis in light of the greater expense of the manual method of brain tumor segmentation. Here, noise reduction was achieved using pre-processing based on wiener filtering (WF). The deep residual U-Net segmentation model and the VGG-19 model were utilized for feature extraction in the ADRU-SCM model. The gated recurrent unit (GRU) model and tunicate swarm optimization (TSO) were used to develop a brain tumor classification model.

Hanene Sahli et al. [35] developed an automatic method for Glioblastoma brain tumor segmentation based on the deep Residual Learning Network (ResNet) to minimize the significant computational power and time consumption. By adding more layers to a deep neural network with a quick training procedure, this method was enhanced. This method uses the fusion method (ResNet-SVM) and obtains an accuracy of 89.36%.

The survey of various related techniques, as well as their performance and limitations, is described in Table 1.

Received: July 18, 2025

International Journal of Applied Mathematics
Volume 38 No. 3s, 2025
ISSN: 1311-1728 (printed version); ISSN: 1314-8060 (on-line version)

Table 1: Analysis of some related techniques

Author name and reference	Technique use	Dataset used	Limitations	Performance
M.O. Khairandish et al. [28]	Hybrid CNN-SVM	BRATS 2015 dataset	Limited features are considered	97.43% accuracy
Ilyasse Aboussaleh et al. [29]	CNN	BraTS 2017 dataset	It only considers FLAIR modalities	91% accuracy
Nagwan Abdel Samee et al. [30]	DCNN	BRATS 2015 dataset	Low performance	88.6% accuracy
R. Pitchai et al. [31]	ANN-Fuzzy K means algorithm	BRATS dataset	It is not affected by over-segmentation	94% accuracy
Angona Biswas and Md. Saiful Islam, [32]	ANN	Figshare dataset	Computation complexity	95.4% accuracy
Amran Hossain et al. [33]	BINet model	Real-time dataset	High computational complexity	89.33% accuracy and 93.10% Dice Score
R. Poonguzhali et al. [34]	TSO-GRU model	FigShare dataset	High time consumption	97.48% accuracy
Hanene Sahli et al. [35]	Combined ResNet-SVM model	MRI dataset	89.36% accuracy	Hard to handle a larger dataset

The requirement for larger datasets renders many strategies for detecting brain tumors less effective. Certain models have a worse overall efficacy for brain tumor identification due to their high computational complexity. While numerous brain tumor classification methods have been created to reduce overfitting in datasets, the training process generates a large amount of noise. Some notable problems encountered while segmenting the MRI image included temporal complexity, high processing costs, and the need for extra parameters. Insufficient identification of dimensions, as well as the location of brain tumors, reduces the efficiency of several methods. Brain tumors frequently exhibit inhomogeneous intensities in their MRI images, which are limited by imaging principles. The MRI image reveals overlapping and unclear borders between the tumor and the surrounding tissues.

Received: July 18, 2025

International Journal of Applied Mathematics
Volume 38 No. 3s, 2025
ISSN: 1311-1728 (printed version); ISSN: 1314-8060 (on-line version)

3. Proposed Methodology

Brain tumors are some of the most serious disorders caused by abnormal cell development in the brain. Removing the tumor from the brain permanently is a challenging task, but it is curable if identified early on. There are three forms of brain tumors: glioma, pituitary, and meningioma. Several techniques were developed to provide effective brain tumor segmentation and classification. However, various drawbacks were observed in brain tumor segmentation and classification, such as low performance, time consumption, computational complexity, and so on. An Effective Multi-modal Brain Tumor Segmentation, as well as Classification method, is presented to address these kinds of problems. Figure 1 outlines the general workflow of the suggested technique.

Initially, the input MRI images, such as T1, T2, and Flair, were extracted from the dataset and pre-processed with Up-MFil, picture scaling, and HSV color channel conversion. It reduces noise and improves image quality. The image is subsequently segmented using the GKT approach to detect a brain tumor. To achieve effective segmentation, the Gannet optimization technique is used to determine the ideal threshold. It is carried out on the basis of the whole tumor (WT), tumor core (TC), and enhanced tumor. From the segmented portions, the needed features are extracted and selected with the aid of the GO_ENetB3 model. Here, the EfficientNet B3 model is responsible for extracting the essential features, and the dimensionality issue is solved by adopting the Enhanced Gannet Optimization (EGO) algorithm. An FT-HDC2Net model is proposed, and the brain tumor disease is recognized and diagnosed based on the features that have been picked. A capsule network and CNN are used to diagnose brain tumor disease. Utilizing the WSO method, the parameters of the suggested classification model are also adjusted.

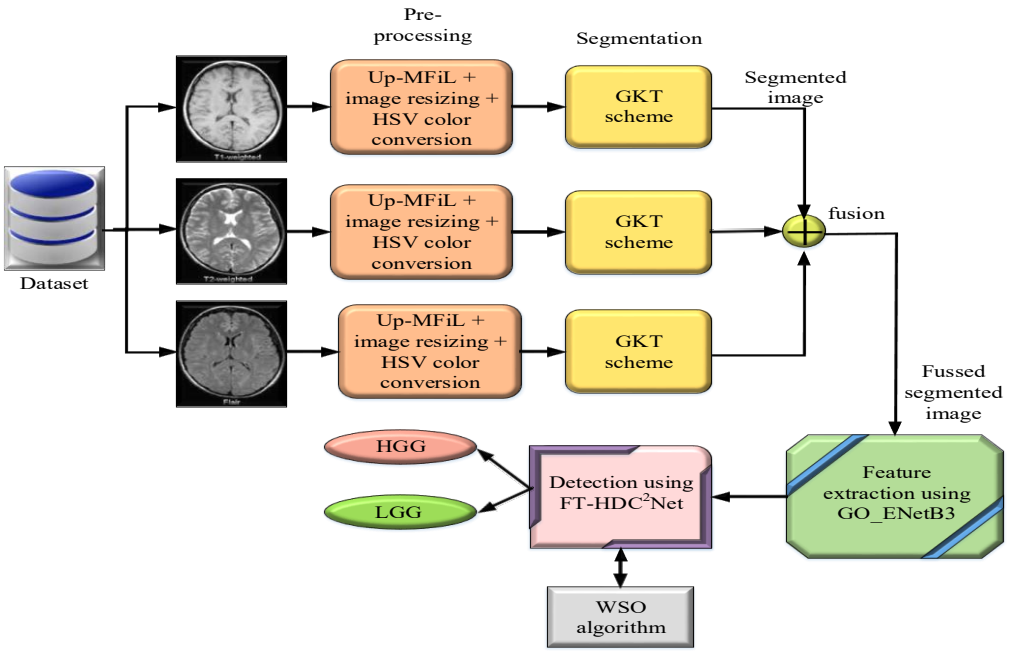

Figure 1: Workflow of proposed methodology

Received: July 18, 2025

International Journal of Applied Mathematics

Volume 38 No. 3s, 2025

ISSN: 1311-1728 (printed version); ISSN: 1314-8060 (on-line version)

3.1 Pre-processing

Image resizing, Up-MFil, HSV color channel conversion, and other techniques are used in the pre-processing stage to minimize noise and increase imaging quality.

3.1.1 Upgraded Mean Filtering

The mean filter with a window size 3×3 is utilized for upgrade mean filtering. Then, it utilized the restricted mean other than the median. Later, it was used for the restricted mean rather than the median. It performs better while evaluating the new gray value for the image's central pixel. The fixed-size window of Advanced Median Filters does not reduce the large noise densities. Hence, the iterative process is incorporated with this technique to reduce the noise from every pixel. The Manhattan distance utilized to end the iterations and the pseudo-code for the Up-MFil method is described in Table 2.

Table 2: Pseudo-code of the Up-MFil technique

Input: Image with noise $I \coloneqq \left[i_{ab}\right]_{x\times y}$

Output: Restored image $J \coloneqq \left[j_{ab}\right]_{x\times y}$

Initializing $s \coloneqq 1, u \coloneqq 0,\ J^{[0]} \coloneqq I, \varepsilon$

Evaluate $\Delta_{Max} \coloneqq Max\left\{j_{ab}\right\}$ and $\Delta_{Min} \coloneqq Min\left\{j_{ab}\right\}$

Repeat $\begin{matrix} 1\le a\le x & 1\le a\le x \\ 1\ge b\ge y & 1\ge b\ge y \end{matrix}$ for each pixel (a,b) of image I^{u} at u stage

if $\left(j_{ab}^{[u]} \ge \Delta_{Max} \,//\, j_{ab}^{[u]} \le \Delta_{Min}\right)$ then,

Define the $R_{ab}^{*}\left(J^{[u]}, s\right)$

Update the $J_{ab}^{h+1} \coloneqq \overline{R}_{ab}^{mean}\left(J^{[h]}, s\right)$

else

Assign the $j_{ab}^{h+1} \coloneqq e_{ab}^{[h]}$

end

end

Until the condition $\left|J^{h+1} - J^{[h]}\right|_1 \le \xi$

Received: July 18, 2025

International Journal of Applied Mathematics

Volume 38 No. 3s, 2025

ISSN: 1311-1728 (printed version); ISSN: 1314-8060 (on-line version)

3.1.2 Image resizing

The process of comprising the pixels of images is known as image resizing, and each pixel in the image has three color combinations such as red, blue, and green. It is used to reduce the size of the image as well as reduce the requirement of many bytes to store the image. The size of the image in the dataset is 512×512 which resized into 400×400 for efficient brain tumour classification.

3.1.3 HSV color channel conversion

This technique is employed to reduce the size of MRI images to avoid classification errors, as shown below.

$$C=\cos^{-1}\frac{\frac{1}{2\left[(R-G)^2+(R-B)\right]}}{\sqrt{(R-G)^2+((R-B)(G-B))}} \tag{1}$$

$$A=1-\frac{3\left[Min(R,G,B)\right]}{R+G+B} \tag{2}$$

$$L=\frac{R+G+B}{3} \tag{3}$$

Here, the Red, Green, and Blue colors are represented as R, G and B. This technique is utilized to trim the edges of each input image, covert the color channel of the image, and improve its quality.

3.2 Segmentation using GKT

The Segmentation stage is used to group pixels based on their similarities and to segment the tumour in an MRI image. Hence, the GKT model was used for segmentation, and its efficiency was improved using Gannet optimization. It is utilized to segment brain tumors based on WT, TC, and ET.

3.2.1 Gannet-based Kapur's thresholding

The segmentation is performed based on a threshold-based technique to evaluate the optimum threshold. The probability distribution and image histogram entropy are required for the calculation. This technique establishes the optimum threshold for entropy. The bi-level threshold is evaluated by objective utility, which is described in the below equation.

$$BTO_{kap}(a)=S_1+S_2 \tag{4}$$

Here, the mathematical expression of S_1 and S_2 described in the equation below.

$$S_1=\sum_{v=1}^{a}\frac{x_v}{e_0}1s\left(\frac{x_v}{e_0}\right) \tag{5}$$

Received: July 18, 2025

International Journal of Applied Mathematics

Volume 38 No. 3s, 2025

ISSN: 1311-1728 (printed version); ISSN: 1314-8060 (on-line version)

$$S_2 = \sum_{v=a+1}^{u} \frac{x_v}{e_1} 1s\left(\frac{x_v}{e_1}\right) \tag{6}$$

Here, the probability distribution D of grayscale intensity level is denoted as x_v for S_1 and S_2 class model. Then, e_0 and e_1 are represented by S_1 and S_2 probability distribution D. The entropy-based model is sufficiently malleable for multilevel thresholding. Here, $s-1$ it is utilized to divide the MRI image into s class labels using the threshold numbers. The variations of objective values are described in the below equation.

$$BTO_{kap}(A) = \sum_{u=1}^{s} S_u \tag{7}$$

Here, a vector involves numerous threshold numbers are represented as $A = [a_1, a_2, a(s-1)]$. The entropies are termed discretely with the corresponding threshold value denoted as a. It is modified for the s entropy, which is described in the below equation.

$$S_s^t = \sum_{x=a_{s+1}}^{K} \frac{xp}{e_{s-1}} 1s\left(\frac{xp}{e_{s-1}}\right) \tag{8}$$

Here, the probability rate for s classes is represented as $(e_0, e_1, ..., e_{s-1})$, and the threshold numbers are optimized utilizing the gannet optimization method.

3.2.2 Gannet optimization algorithm

A metaheuristic Gannet optimization algorithm was utilized to regulate the optimal threshold for efficient segmentation [36]. The mathematical expression to update the position is described in the below equation.

$$GO_a(y+1) = \begin{cases} O_a(y) + p_1 + p_2, & n \geq 0.5 \\ O_a(y) + q_1 + q_2, & n < 0.5 \end{cases} \tag{9}$$

$$p_2 = R * (O_a(y) - O_a(y)) \tag{10}$$

$$q_2 = Q * (O_a(y) - O_a(y)) \tag{11}$$

$$R = (2 * i_4 - 1) * h \tag{12}$$

$$Q = (2 * i_5 - 1) * t \tag{13}$$

Here, the random numbers between 0 and 1 are represented as i_4 and i_5. The random number between $-h$ as well as h is described as p_1, similarly, the random number among $-t$ as well as t is represented as q_1. The a^{th} distinct in current inhabitants is denoted as $O_a(y)$. Then, $O_i(y)$

Received: July 18, 2025

International Journal of Applied Mathematics
Volume 38 No. 3s, 2025
ISSN: 1311-1728 (printed version); ISSN: 1314-8060 (on-line version)

and $O_k(y)$ are arbitrarily selected distinct and average locations of distinct in the current inhabitants, which is described in the below equation.

$$O_k(y)=\frac{1}{Z}\sum_{a=1}^{Z}O_a(y) \tag{14}$$

Here, Gannet-based Kapur's Thresholding is utilized to perform segmentation based on intensity, texture, or color. The Gannet optimization is utilized to choose the optimal threshold to provide efficient segmentation.

3.3 Feature extraction and selection performed by the GO_ENetB3 model

The feature extraction is performed by the GO_ENetB3 model, which is the combination of the EfficientNet B3 model and the EGO algorithm. In this technique, the EfficientNet B3 model is utilized to remove the features, and the EGO algorithm is utilized to select optimal features and solve the dimensionality issues.

3.3.1 Feature extraction using EfficientNetB3

The EfficientNet is a type of CNN that includes several convolutional layers, such as Mobile Inverted Residual Bottleneck Convolutional (MBConv) blocks and fully connected layers. The Efficient is smaller than other models, such as ResNet50 and EfficientNet-B0, which includes 23,534,592 and 5,330,564 boundaries. These models have high computational power; hence, EfficientNetB3 is utilized to extract the features [37].

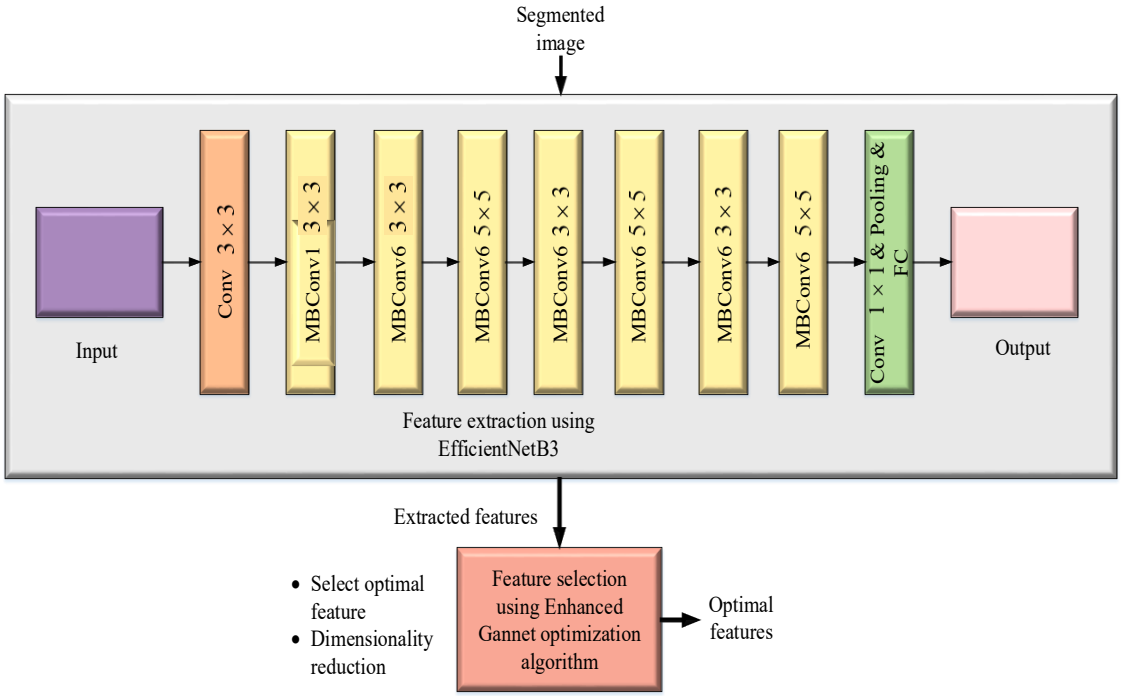

Figure 2: Architecture of GO_ENetB3 model

Received: July 18, 2025

International Journal of Applied Mathematics

Volume 38 No. 3s, 2025

ISSN: 1311-1728 (printed version); ISSN: 1314-8060 (on-line version)

MBConv is the fundamental component of the EfficientNet paradigm and is included in MobileNet-V2. Initially, the EfficientNet model employs a stem architecture, which is shared by all eight models and their final layers. There are seven blocks available, each with a unique sub-block. It moved from the EfficientNetB0 to the EfficientNetB7 model by increasing the number of iterations. EfficientNetB0 and EfficientNetB7 each have 237 and 813 layers, respectively. The second module finds the first sub-block of seven main blocks, with the exception of the first block. The skip connection connects Module 3 to each sub-block, and it is the first sub-block to be merged with Module 4. In Module 5, each sub-block is connected to the one behind it using a skip path. Finally, these modules are merged and used in precise ways within the blocks to form sub-blocks. The architecture of the GO_ENetB3 model utilized for feature extraction, as well as optimal feature selection, is represented in Figure 2.

3.3.2 Feature selection using EGO algorithm

The Gannet optimization algorithm (GoA), a metaheuristic optimization method, was replaced by the EGO. It takes its cues from the gannet bird's natural predation behavior, which emulates the concepts of genetic inheritance and fittest survival to gradually evolve the population of solutions toward the ideal or nearly ideal state. There are two phases to it: exploration and exploitation. The mechanism operates on the basis of abrupt rotation, random wandering, and U-shaped and V-shaped diving modes.

3.3.2.1 Initialization

The population of potential solutions is randomly generated by every individual. These individuals denote the possible solution for optimization issues. The initial population is assumed by the gannets, which are initialized randomly with the boundary values, and it is described in the below equation.

$$g_{x,y} = rand_1 \times \left(B_y - b_y\right) + b_y \tag{15}$$

here, $g_{x,y}$ represents the position of x^{th} the search agent in y^{th} dimension. Then, B_y and b_y are denoted as upper and lower boundaries. The random value is denoted as $rand_1$ which lies between 0 and 1.

The memory matrix is represented by the term YM in this process; the gannet's position is changed over the iteration, which is returned in the memory matrix. The matrix value is modified based on the fitness measurements.

3.3.2.2 Exploration

During the exploration phase, gannets search the water's surface for prey. Then, it adjusts their diving patterns to match the water depth. U-shaped and V-shaped dives are the two different forms, as the equation below illustrates.

$$U = 2 * \cos(2 * \pi * srand_2) * g \tag{16}$$

Received: July 18, 2025

International Journal of Applied Mathematics

Volume 38 No. 3s, 2025

ISSN: 1311-1728 (printed version); ISSN: 1314-8060 (on-line version)

$$V = 2 * P\left(2 * \pi * srand_3\right) * g \tag{17}$$

$$g = 1 - \frac{gc}{gm} \tag{18}$$

In equation (18), the maximum iteration count and current iteration are represented as gm and gc. Then, $srand_2$ and $srand_3$ are denoted as random values that lie between 0 and 1. The updated position based on two dive criteria is described in the below equation.

$$D_j(g+1) = \begin{cases} D_j(g) + S_1 + S_2, & x \geq 0.5 \\ D_j(g) + T_1 + T_2, & x < 0.5 \end{cases} \tag{19}$$

here, $S_2 = u * \left(D_j(g) - D_h(g)\right)$ and $T_2 = u * \left(D_j(g) - D_s(g)\right)$.

The mathematical expression for terms u and v are described in the below equation.

$$u = (2 * srand_4 - 1) * U, \; v = \left(2 * srand_5 - 1\right) * V \tag{20}$$

Here, random values between 0 and 1 are denoted as the variables $srand_4$ and $srand_5$. Then, $D_j(g)$ denotes the current search agent and $D_h(g)$ represented a random selection of the population. The average position is denoted as $D_S(g)$ correspondingly, and the evaluation of the average position is described in the below equation.

$$D_S(g) = \frac{1}{L} \sum_{j=1}^{L} D_j(g) \tag{21}$$

3.3.2.3 Exploitation

The gannet catches the prey after the search agents rush to the surface of the water, which requires more energy. The enormous energy is utilized by the gannets to capture the prey. The gannet can effectively catch its prey when it is supplied with enough energy. Based on the strategy of capturing, the updated position is described in the below equation.

$$D_j(g+1) = \begin{cases} g * \delta * \left(D_j(g) - D_{bt}(g)\right) + D_j(g), & Rx \geq c \\ D_{bt}(g) - \left(D_j(g) - D_{bt}(g)\right) * M * g, & Rx < c \end{cases} \tag{22}$$

here, c denotes the constant parameters, which are fixed as 0.2, and the term Rx is evaluated based on the below-described equation.

$$Rx = \frac{1}{X * g2} \tag{23}$$

$$g2 = 1 + \frac{gc}{gm} \tag{24}$$

Received: July 18, 2025

International Journal of Applied Mathematics

Volume 38 No. 3s, 2025

ISSN: 1311-1728 (printed version); ISSN: 1314-8060 (on-line version)

$$X = \frac{mS * eS^2}{d} \tag{25}$$

$$d = 0.2 + (2 - 0.2) * srand_6 \tag{26}$$

here, $srand_6$ denotes the random value between 0 to 1, and mass as well as the velocity of the gannet is represented as mS as well as eS , which is set to be 2.5 Kg and 1.5 m/s. The mathematical expression of the term δ is shown below.

$$\delta = Rx * \left| D_j(g) - D_{bt}(g) \right| \tag{27}$$

$$M = Levy(K) \tag{28}$$

Here, the best value is obtained, and this algorithm is improved to identify the issues of optimizing transportation and placing pooling centers. The EGO algorithm is utilized to improve the performance by finding the optimum value. The conventional GoA method is integrated to evaluate the new equation. The GoA eliminates the problems with local optima and offers good processing capability and a higher convergence rate. However, the GoA yields extra complexity by employing a large number of parameters to lower the EGO. The major issues of GoA are parameter setting and its adaptation. Hence, the delta parameter derived from equation (22) is replaced with the below-described equation.

$$\delta = \frac{\beta}{\gamma} \tag{29}$$

$$\gamma = \frac{\beta}{\alpha} \tag{30}$$

Here, the mathematical expression for the term α and β is described in the equation below.

$$\alpha = \frac{L}{100} \tag{31}$$

$$\beta = \frac{L}{20} \tag{32}$$

Here, the total number of the population is denoted as the term L . Hence, the updated or modified delta value is utilized in the equation (22) to obtain a better solution. The pseudo-code of the EGO algorithm is represented in Table 3.

Received: July 18, 2025

International Journal of Applied Mathematics

Volume 38 No. 3s, 2025

ISSN: 1311-1728 (printed version); ISSN: 1314-8060 (on-line version)

Table 3: Pseudo-code of EGO algorithm

Let's assume input search agents as well as total iteration
Evaluate memory matrix
Find the value of fitness
while
for each value in the memory matrix
if $x \geq 0.5$
update the gannet's location utilizing equation (18)
else
update the gannet's location utilizing equation (18)
end if
if $c \geq 0.2$
Evaluate the term δ using equation (29) – (32)
Analyze the location of the gannet using equation (22)
else
Analyze the location of the gannet using equation (22)
end while
Return optimum value

3.4 Classification using FT-HDC²Net

The brain tumor is classified into glioma, pituitary, and meningioma tumors using the FT-HDC2Net model, which is a combination of the CNN and capsule networks. Then, the hyperparameter utilized in the model is tuned using the WSO algorithm.

3.4.1 CNN

The multidimensional data, which includes the pooling layer, convolutional layer, and ReLU layer used in this model, is processed by CNN [38]. From the preceding layers, the convolutional layer is used to ascertain the local connectivity of the feature. It also maps their information in a specific feature map. The convolution of input X with filter L $\left(F \in \Re^{2p_1+2p_2}\right)$ which is shown below.

$$\left(X * L\right)_{a,b} = \sum_{h=-p_1}^{p} 1 \sum_{k=-p_2}^{p} 2L_h, \quad {}_kX_{a-h,b-1} \tag{33}$$

Received: July 18, 2025

International Journal of Applied Mathematics

Volume 38 No. 3s, 2025

ISSN: 1311-1728 (printed version); ISSN: 1314-8060 (on-line version)

here, $\mathrm{Re}\,LU\ (Q(d)=\max(0,\,d))$ denotes the non-linearity activation function, which is utilized to generate feature maps with convolutional layers. Similar features are combined using the max-pooling layers conveyed from the previous layer. The downsampling operation is carried out by the max-pooling layers by determining the maximum value of every field that overlaps the filter on the feature map.

The CNN structure from the fully connected (FC) layer to the classification is similar to the multilayer perceptron neural network (MLP). In the MLP layer, the process of both the FC layer and the hidden layer are the same. CNN structure includes one or more FC layers, and it connects the neuron in the next layer to the previous layer. The non-normalized values of the previous layer in CNNs are usually matched to a probable distribution across projected class scores using the softmax function. The following equation describes the mathematical role of the CNN's softmax function.

$$\sigma(i_n)=\frac{e^{i_n}}{\sum_{m=1}^{H}e^{i_n}},\qquad m=1,2,\ldots,H \tag{34}$$

Here, softmax output for every i_n is represented by $\sigma(i_n)$, and the values of the input vector are denoted as i_m.

The training time of CNNs is reduced using the batch normalization layers and sensitivity to the network initialization. Hence, the normalization process is selected for this layer. The normalized activations with input i_n, mini-batch mean B_M, and mini-batch variance B_V are evaluated using the below-described equation.

$$\hat{i}_n=\frac{i_n-B_M}{\sqrt{B_V^2+t}} \tag{35}$$

Here, the constant is represented as t which develops the numerical state when B_V is very small. The mathematical equations of B_M and B_V are described in the below equations.

$$B_M=\frac{1}{a}\sum_{x=1}^{a}i_n \tag{36}$$

$$B_V=\frac{1}{a}\sum_{i=1}^{a}(i_n-B_M)^2 \tag{37}$$

Finally, it calculates the activations in the batch normalization layer using shift, and the mathematical description of the scale operation is shown in the equation below.

$$j_n=x\hat{i}_n+y \tag{38}$$

Received: July 18, 2025

International Journal of Applied Mathematics

Volume 38 No. 3s, 2025

ISSN: 1311-1728 (printed version); ISSN: 1314-8060 (on-line version)

Here, the balance and scale factors are represented as x and y . During the training process, these factors are learnable variables that are utilized to update the most appropriate values. The vectorial formulation has the ability to provide a capsule to identify features and also recognize changes to be a feature. It is an important property that distinguishes the capsule as an effective but lightweight feature representation approach.

3.4.2 Capsule Network

The vectorial capsule representations serve as the core neurons in capsule networks, which describe the features of entities. More exactly, a capsule's starting parameters describe the entity's inherent characteristics, but the capsule's length represents the entity's probability of existence. Conventional convolution procedures and capsule convolution processes are very different from one another. The entire input to a capsule y in a capsule's convolution layer. The mathematical equation for the total input to the capsule is described below.

$$A_y = \sum_x p_{xy} \cdot U_{xy} \tag{39}$$

Here, total input to the capsule y is denoted as A_y. The coupling coefficient is dynamically determined as p_{xy} , which indicates the contribution degree of prediction from the capsule x in the previous layer. The prediction form capsule x is represented as U_{xy} which is described in the below equation.

$$U_{xy} = V_{xy} \cdot U_x \tag{40}$$

Here, the output of the capsule x is represented as U_x , and the transformation matrix acts as a feature mapping function is represented as V_{xy}. For instance, all the connected capsules of the capsule x in the layer have coupling coefficients that add up to 1. The enhanced dynamic routing process is utilized to determine the coupling coefficients, which are effectively utilized to construct a deep capsule network.

According to the length-based probability encoding method, capsules that are used more often should forecast with greater probability, while shorter capsules should contribute less to probability estimations. Lastly, to normalize the capsule's output, the squashing function is used as an activation function. The following equation describes the squashing function's mathematical expression.

$$U_y = \frac{\|A_y\|^2}{1+\|A_y\|^2} \cdot \frac{A_y}{\|A_y\|} \tag{41}$$

Here, the original input, as well as the normalized output of the capsule, y are represented as A_y and U_y. By normalizing, long capsules are shrunk to a length close to one, casting high

Received: July 18, 2025

International Journal of Applied Mathematics
Volume 38 No. 3s, 2025
ISSN: 1311-1728 (printed version); ISSN: 1314-8060 (on-line version)

predictions. In contrast, short capsules are repressed to almost zero length to provide fewer contributions. Figure 3 illustrates the FT-HDC2Net model's architecture.

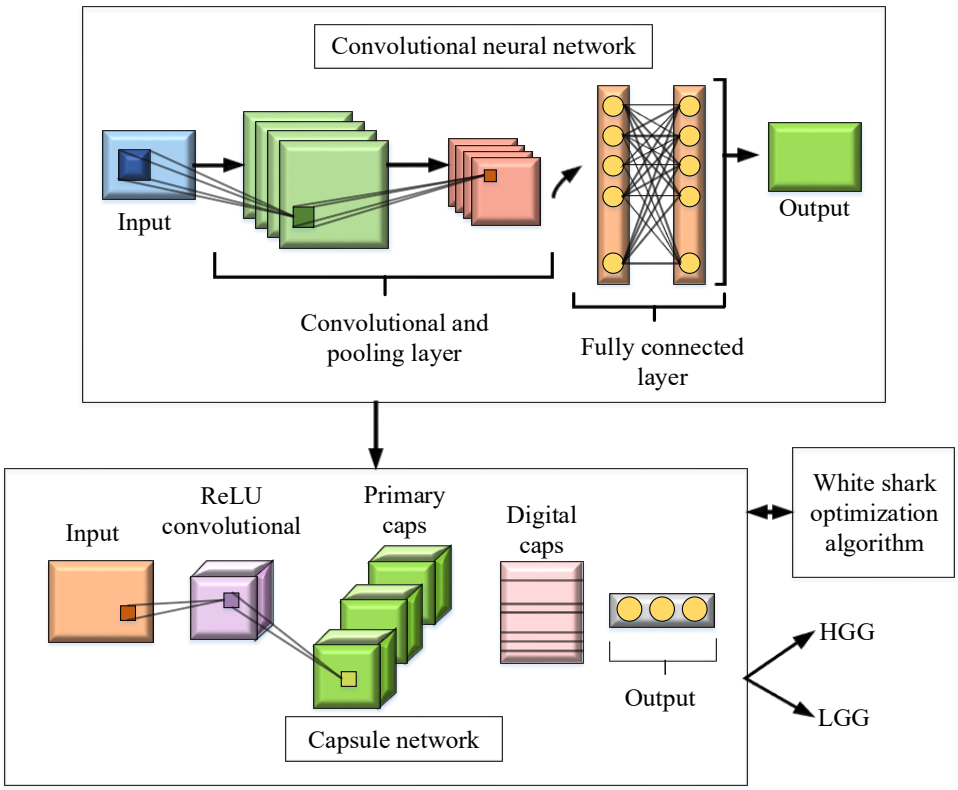

Figure 3: Architecture of FT-HDC^{2}Net model

3.4.3 Hyperparameter tuned using WSO algorithm.

The hyperparameters are tuned using the WSO method and are modeled after the hunting and tracking behaviors of white sharks during foraging [39].

3.4.3.1 Initialization

The WSO is a population-based method that generates a pool of starting solutions to optimization problems at random to start the optimization process. The population of n white sharks in d-dimensional search space with every white shark's position is known as the candidate solution of the problem. It can be described mathematically in $2d$ the matrix, as shown below in the equation.

$$s = \begin{bmatrix} s_1^1 & s_2^1 & \cdots & \cdots & s_d^1 \\ s_1^2 & s_2^2 & \cdots & \cdots & s_d^2 \\ \vdots & \vdots & \vdots & \vdots & \vdots \\ s_1^x & s_2^x & \cdots & \cdots & s_d^x \end{bmatrix} \tag{42}$$

Here, the location of every white shark in the search space is denoted as s , and the amount of decision variables is represented as d. Then, the position of i^{th} the white shark in d^{th} is

Received: July 18, 2025

International Journal of Applied Mathematics

Volume 38 No. 3s, 2025

ISSN: 1311-1728 (printed version); ISSN: 1314-8060 (on-line version)

denoted as s_d^i . The equation below describes the uniform random initialization used to generate the initial population in the search domain.

$$s_j^i = h_j + rand \times \left(UB_j - LB_j\right) \tag{43}$$

Here, the initial vector of i^{th} the white shark in j^{th} dimension is represented as s_j^i . The upper as well as lower bounds of search space in j^{th} dimension is denoted as UB_j as well as LB_j . Then, the random number generated in the interval [0, 1] is represented as $rand$.

Every candidate solution for a white shark's new position is evaluated according to a fitness function. The former is renovated if it is determined that the new position is superior to the current one. If the white shark's current position in the WSO simulation is better than its new position, then it will stay in the current position.

3.4.3.2 Speed movements toward the prey

Since white sharks are creatures with a need to survive, they spend a great deal of time hunting and pursuing prey. They generally use all available techniques, such as extraordinary senses of smell, sight, and hearing, to track and track their prey. A white shark swims in an erratic rhythm in search of its prey, identifying it by listening for waves to break while it is moving. The mathematical equation for the velocity vector is described below.

$$c_{l+1}^i = \mu\left[c_l^i + f_1\left(s_{gbest_l} - s_l^i\right) \times u_1 + f_2\left(s_{best}^{c_l^i} - s_l^i\right) \times u_2\right] \tag{44}$$

Here, the index of white sharks for a population size x is represented as $i = 1,2,\ldots,x$. The new velocity vector of i^{th} the white shark in $\left(l+1\right)^{th}$ step is represented as c_{l+1}^i . The current speed vector of i^{th} the white shark in l^{th} step is represented as c_l^i . The global optimal location vector is attained by the shark in l^{th} iteration and is denoted as s_{gbest_l} . The existing location of i^{th} the white shark in l^{th} the step is represented as $s_{best}^{c^i}$, and the i^{th} index vector of white sharks is denoted as c^i , which searches the optimal position using the equation (45). Here, the two uniformly generated random numbers are represented as u_1 and u_2 . The force of white sharks is represented as f_1 and f_2 which utilized to control the effect of s_{gbest_l} and $s_{best}^{c^i}$ on s_l^i using (46) and (47). The constriction factor is represented as μ which utilized to analyze the shark's convergence behavior using equation (48).

$$c = \left[x \times R(1,\ x)\right] + 1 \tag{45}$$

Here, the vector of a random number generated with uniform distribution in the range [0, 1] is represented as $R(1, x)$.

Received: July 18, 2025

International Journal of Applied Mathematics

Volume 38 No. 3s, 2025

ISSN: 1311-1728 (printed version); ISSN: 1314-8060 (on-line version)

$$f_1 = f_{\max} + \left(f_{\max} - f_{\min}\right) \times e^{-(4l/L)^2} \tag{46}$$

$$f_2 = f_{\min} + \left(f_{\max} - f_{\min}\right) \times e^{-(4l/L)^2} \tag{47}$$

Here, existing as well as the total number of the iterations are represented as l and L. The initial and subordinate velocities are represented as $f_{\min}$ and $f_{\max}$ utilized to achieve better motion for white sharks. After rigorous analysis, the values of $f_{\min}$ and $f_{\max}$ are set to be 0.5 and 1.5.

$$\mu = \frac{2}{\left|2 - \tau - \sqrt{\tau^2 - 4\tau}\right|} \tag{48}$$

Here, the acceleration coefficient is denoted as τ is equal to 4.125.

3.4.3.3 A movement toward optimal prey

White sharks spend most of their time seeking prey that are either ideal or suboptimal. The white sharks constantly change postures and travel towards the prey based on the wave created by the prey and its smell. Sometimes, the prey escapes from the white shark when the prey moves based on the flow of waves. The white shark can track the prey by its smell even when it leaves their position. A white shark's approach to searching for prey in random locations is comparable to how fish schools search for food. The white shark's approach to prey is characterized by the position-updating strategy outlined in the equation below.

$$s_{l+1}^i = \begin{cases} s_l^i \cdot \neg \oplus s_0 + UL \cdot p + LL \cdot q; & R < mf \\ s_l^i + c_l^i / w; & R \geq mf \end{cases} \tag{49}$$

Here, the Updated position vector of i^{th} the white shark in $(l+1)^{th}$ the iteration step is represented as s_{l+1}^i and the negation operator is denoted as $\neg$. The one-dimensional binary vectors are denoted as p well as q, which is determined by the equations (50) and (51). Equation (52) was utilized to evaluate the frequency of wavy motion in white sharks. The random number generated in the range [0, 1] is denoted as R, and the movement force is denoted as mf, which increases with the number of iterations. It is performed by the white shark approaching prey, and it is described in the equation below.

$$p = \operatorname{sgn}\left(s_l^i - UL\right) > 0 \tag{50}$$

$$q = \operatorname{sgn}\left(s_l^i - LL\right) < 0 \tag{51}$$

$$s_0 = \oplus\left(p,\ q\right) \tag{52}$$

Here, a bit-wise xor operation is represented as $\oplus$.

Received: July 18, 2025

International Journal of Applied Mathematics

Volume 38 No. 3s, 2025

ISSN: 1311-1728 (printed version); ISSN: 1314-8060 (on-line version)

In order for support solutions to behave randomly in the search space, these equations (50) and (51) must be satisfied. It is also utilized to assist the shark in searching every potential area of search space.

$$w = w_{Min} + \frac{w_{Max} - w_{Min}}{w_{Max} + w_{Min}} \tag{53}$$

Here, minimum as well as maximum frequencies of the rolling signal are represented as w_{Min} and w_{Max}. A random number is represented as R. Then, w_{Min} and w_{Max} value is set to be 0.07 and 0.75 to handle the problem. These numbers can be readily altered for different situations when necessary because they were selected with thorough research and testing for a variety of problems.

$$mf = \frac{1}{\left(p_0 + e^{(H/2-h)/p_1}\right)} \tag{54}$$

Here, the two positive constants are represented as p_0 and p_1 which are used to manage both exploration as well as exploitation phases. Then, a parameter mf utilized to determine the white shark's strength for hearing, sense as well as smell.

3.4.3.4 A movement toward the best white shark

When the white shark is near its prey, it maintains its position. The equation below describes how this behavior occurs.

$$s'^{i}_{k+1} = s_{gbest_l} + rand_1 \vec{I}_s \operatorname{sgn}(rand_2 - 0.5) \qquad rand_3 < g_g \tag{55}$$

Here, the updated position of i^{th} white sharks based on the position of prey is denoted as s'^{i}_{l+1}. Then, $(rand_2 - 0.5)$ gives either 1 or -1 to modify the search direction; the random numbers are denoted as $rand_1$, $rand_2$ and $rand_3$ which lies among [0, 1]. The distance between the prey as well as the white shark is represented as $\vec{I}_s$ using equation (56). The parameter is denoted as g_g to determine the white shark's strength for smell and sight when it went close to the optimal prey, which is described in equation (57).

$$\vec{I}_s = \left| R \times \left(s_{gbest_l} - s^i_l \right) \right| \tag{56}$$

The random number is represented as R lies in the range of [0, 1], as well as the current position of white share based on s_{gbest_l} is represented as s^i_l.

$$u_u = \left| 1 - e^{(-p_2 \times h/H)} \right| \tag{57}$$

Received: July 18, 2025

International Journal of Applied Mathematics

Volume 38 No. 3s, 2025

ISSN: 1311-1728 (printed version); ISSN: 1314-8060 (on-line version)

Here, the positive constant is represented as p_2 which is used to control both exploration as well as exploitation, and it is set to be 0.0005 for every addressed test problem.

3.4.3.5 Fish school behavior

Maintain the top two optimal solutions and adjust the placements of the remaining sharks according to the best positions determined by analyzing the behavior of white sharks in groups. The following equation describes the mathematical behavior of fish groups in white sharks.

$$s_{l+1}^{i} = \frac{s_{l}^{i} + s_{l+1}^{\prime i}}{2 \times R} \tag{58}$$

Here, a random number distributed frequently within the interval [0, 1] is denoted as R. Equation (57) is used to update shark positions so that they are in line with the ideal white shark position, which is close to the prey.

At some point, great white sharks may locate themselves inside the search space, often in close proximity to the best prey. The behavior of fish schools and the migration of white sharks to the best white sharks can be used to predict the collective behavior of WSO, which raises the possibility of more aspects of exploration and exploitation.

3.4.3.6 Exploration phase

Some of the parameters utilized for the exploration are described as follows.

μ : It is utilized to control exploration behavior, avert early convergence, as well as prevent the solution from descending into local optima. Its value depends on the parameter τ.

f_1 as well as f_2 : These parameters, which are iteration functions that determine the velocity of white sharks, will be adjusted during WSO's global and local searches to ensure an equal balance of exploration and exploitation. WSO's global and local searches, which are iteration-dependent parameters, control the white sharks' velocity updates and maintain a constant balance of exploration and exploitation. Therefore, during the WSO iterations, these parameters are flexible to enable reasonable exploration ability with accurate results.

mf : This parameter was chosen based on experimental assessments; it shouldn't be greater than 1.0 as this would result in a decline in exploration performance. In the initial iterations, all white sharks are found far from their target. Using mf to update the location of white sharks based on equation (50) facilitates both local and global space searching for WSO. The stronger the exploration capability as well as the higher the coefficient p_1 in mf. Similarly, a lower $a0$ indicates a better capability for exploitation and a low capacity for exploration. Due to this, the value was appropriately adjusted to increase the capabilities for both exploration and exploitation. Based on test results, it is discovered that values that are primarily greater than 20 for p_0 and more than 100 for $a1$ promote search agents to look for boundaries.

Received: July 18, 2025

International Journal of Applied Mathematics

Volume 38 No. 3s, 2025

ISSN: 1311-1728 (printed version); ISSN: 1314-8060 (on-line version)

$\mathrm{sgn}(rand_2 - 0.5)$ In Equation (55): It is utilized to control the direction of exploration $rand_2$.

$rand_1$ In Equation (55): It is utilized to assist the solution in searching space randomly, and variable variation provides efficient exploration.

3.4.3.7 Exploitation phase

Some parameters utilized to control exploitation and location search are described as follows.

μ : It is utilized for an intensity amount of exploitation, and its value relies on the parameter τ that reduces the likelihood of slack in local optima solutions.

f_1 and f_2 : These factors affect WSO's performance, which is demonstrated by their efforts to strike a balance between local and global search activity.

mf : Exploration decreases, and exploitation increases with the number of iterations. In the final iterations, when a white shark is close to a prey, mf will assist the WSO in executing a local search for the prey, which will result in exploitation. Additionally, the exploitation feature of mf is controlled by coefficients a0 and a1. By creating around the optimal answer, it determines the extent of exploitation.

$\mathrm{sgn}(rand_2 - 0.5)$ in equation (56): It controls exploitation by determining the local search's direction since, $rand_2$ because it exists in [0, 1], there is an equal chance of positive and negative signs.

$rand_1$ in equation (56): It enhances the search space's solution uncertainty, enabling a sensible exploitation process.

3.4.3.8 Complexity analysis

The computational complexity of an algorithm can be represented as a function that links the method's run-time to the size of the input required to solve the problem. This is accomplished by utilizing the well-known Big-O notation, which is explained below, to calculate the computational complexity of the WSO in both time and space.

Time complexity

This complexity problem formed based on the number of white sharks x, the number of iterations H , the given problem's dimension d , and the cost of function assessment u_2 . The mathematical equation for the time complexity of WSO is described below.

$$C(wso) = C(prob.def) + C(init.) + (\cos t\ function) + (U\_sol) \tag{59}$$

Here, the component's time complexity is described in equation (60), which is described as follows.

Initializing the problem definition demands $C(1)$ time.

Received: July 18, 2025

International Journal of Applied Mathematics

Volume 38 No. 3s, 2025

ISSN: 1311-1728 (printed version); ISSN: 1314-8060 (on-line version)

Initialized population generation demands $C(x \times d)$ time.

Assess cost function demands $C(H \times u \times x)$ time.

Calculate updated solution demands $C(H \times u \times d)$ time.

Based on these, the total time complexity of WSO is described in the equation below.

$$C(wso) = C(1 + xd + Hux + Hxd) \tag{60}$$

As $1 << Hux, 1 << Hud, xd << Hux$ and $xd << Hux$, then equation (60) is reduced to equation (61).

$$C(wso) \cong C(Hux + Hxd) \tag{61}$$

It clearly defines the WSO's time complexity as polynomial order.

Space complexity

The parameters for the number of white sharks, as well as the problem's dimensions, determine the WSO's space complexity in relation to memory space. This indicates the amount of space needed for the planned WSO's initialization.

$$C(xd) \tag{62}$$

The pseudo-code summarizing the iterative optimization process of the WSO algorithm is described in Table 4.

Table 4: Pseudo code of WSO algorithm

Initialize problem parameter

Initialize parameter of WSO

Generate the initial position of WSO randomly

Initialize velocity of every initial population

Evaluate its position

while $h < H$ **do**

Update $c, u_1, u_1, p, q, s_o, w, mf$ *and* g_g using equation (45), (46), (47), (48), (50), (51), (52), (53), (54) and (57)

for $i = 1$ *to* x **do**

$$c_{l+1}^{i} = \mu\left[c_l^i + f_1\left(s_{gbest_l} - s_l^i\right) \times u_1 + f_2\left(s_{best}^{c_l^i} - s_l^i\right) \times u_2\right]$$

end for

for $i = 1$ *to* x do

Received: July 18, 2025

International Journal of Applied Mathematics

Volume 38 No. 3s, 2025

ISSN: 1311-1728 (printed version); ISSN: 1314-8060 (on-line version)

if $R < mf$ **then**

$$s_{l+1}^{i} = s_{l}^{i} \cdot \neg \oplus s_0 + UL \cdot p + LL \cdot q$$

else

$$s_{l+1}^{i} = s_{l}^{i} + c_{l}^{i} / w$$

end if

if $R < g_g$ **then**

$$s_{l+1}^{i} = s_{gbest_l} + rand_1 \vec{I}_s \operatorname{sgn}(rand_2 - 0.5)$$

else

$$s_{l+1}^{\prime i} = s_{gbest_l} + rand_1 \vec{I}_s \operatorname{sgn}(rand_2 - 0.5)$$

$$s_{l+1}^{i} = \frac{s_{l}^{i} + s_{l+1}^{\prime i}}{2 \times R}$$

end if

end if

end for

adjust white sharks' position beyond the boundaries

calculate and update the new position

$h = h + 1$

end while

Return optimal solution

4. Result

Several similar techniques, including CNN, Residual Network (ResNet) 18, Long Short-Term Memory (LSTM), and AlexNet, were used to examine the overall performance of the suggested method. A number of performance indicators are used to evaluate the effectiveness of the strategies examined. The effectiveness of the suggested technique is expressively described when contrasted with the performance of the current model.

4.1 Dataset description

The multi-modal brain tumor image segmentation benchmark (BRATS) dataset 18 was utilized in the proposed technique. It includes various images gathered from 285 glioma patients. Nearly 210 images are HGG, and the remaining images belong to the LGG cases. BraTS 2018 includes

Received: July 18, 2025

International Journal of Applied Mathematics

Volume 38 No. 3s, 2025

ISSN: 1311-1728 (printed version); ISSN: 1314-8060 (on-line version)

66 patients with unknown grades. The storage capacity of this dataset is 28.95 GB, the usability of the proposed technique is 1.88, and it is the publicly available dataset. The training data's ground truth is labeled by the expert, which is not a publicly available dataset. This dataset includes four main classes: Enhancing tumor, Edema, Healthy tissue, and Necrosis/non-enhancing tumor. This BraTS dataset 2018 dataset can be assessed through https://www.kaggle.com/datasets/sanglequang/brats2018.

4.2 Performance metric and its formulation

The overall performance of the proposed technique analyzed its performance using various performance metrics with its formulation are described as follows.

4.2.1 Accuracy

Accuracy is the performance metric utilized to evaluate the accurate detection of the model, which is described below.

$$accuracy = \frac{tp + tn}{tp + fp + tn + fn} \tag{63}$$

Here, the measurement of true positive and true negative are represented as tp and tn. The values of false positive as well as false negative are denoted as fp as well as fn.

4.2.2 Precision

The performance parameter known as precision is evaluated using the equation that follows, which represents the ratio of positive prediction to total positive prediction.

$$precision = \frac{tp}{tp + fp} \tag{64}$$

4.2.3 Recall

The ratio of positive prediction analyzed based on the sum of true positives as well as false negative prediction is known as recall or sensitivity, which is described in the equation below.

$$recall = \frac{tp}{tp + fn} \tag{65}$$

4.2.4 F1-score

F1-score is measured based on the average precision and recall, which is described in the equation below.

$$F1 = \frac{precision \times recall}{precision + recall} \tag{66}$$

4.2.5 Specificity

Received: July 18, 2025

International Journal of Applied Mathematics

Volume 38 No. 3s, 2025

ISSN: 1311-1728 (printed version); ISSN: 1314-8060 (on-line version)

Specificity is a performance utilized to evaluate the ratio of actual negative cases from correctly predicted data, which is described in the below equation.

$$specificity = \frac{tn}{tn + fp} \tag{67}$$

4.2.6 Kappa

According to the equation below, the Kappa factor is defined as the ratio of the difference between the chance of random agreement and the possibility of agreement.

$$\kappa = \frac{d_o - d_e}{1 - d_e} \tag{68}$$

Here, the probability of observed agreement is denoted as d_o , and the probability of agreement by change is represented as d_e.

4.2.7 MAE

The Mean Absolute Error (MAE) is evaluated as the difference between the actual as well as predicted value, which is described in the below equation.

$$mae = \frac{1}{x} = \sum_{i=1}^{x} \left(e_1 - \hat{e}_i \right) \tag{69}$$

Here, the actual and predicted values are represented as e_i and $\hat{e}_i$.

4.2.8 MSE

The Mean Square Error (MSE) evaluates the average square difference between actual and predicted values, which is shown below.

$$mse = \frac{1}{x} = \sum_{i=1}^{x} \left(e_1 - \hat{e}_i \right)^2 \tag{70}$$

4.2.9 RMSE

The root mean square error (RMSE) is the square root of MSE, which is described in the equation below.

$$rmse = \frac{1}{x} = \sum_{i=1}^{x} \left(e_1 - \hat{e}_i \right)^2 \tag{71}$$

4.3 Performance evaluation of the proposed technique

The overall performance of the suggested technique was analyzed using various related techniques, such as LSTM, ResNet18, AlexNet, and CNN. By contrasting it with these methods, the suggested technique's effective performance is explained. The comparison of

Received: July 18, 2025

International Journal of Applied Mathematics
Volume 38 No. 3s, 2025
ISSN: 1311-1728 (printed version); ISSN: 1314-8060 (on-line version)

accuracy, precision, and recall utilizing the suggested and related methodologies is shown in Figure 4.

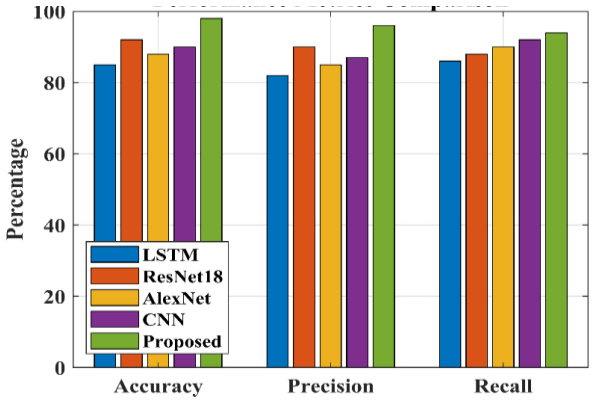

Figure 4: Comparison of Accuracy, Precision and Recall

Initially, accuracy, precision, as well as recall of the proposed technique, were analyzed, and different existing techniques were compared to determine efficient performance. Figure 4 clearly shows that the suggested method achieves higher accuracy than other related methods. The proposed method achieves 98% accuracy, 96.52% precision, and 94.03% recall. The proposed technique provides efficient brain tumor segmentation and prediction by achieving this performance. The accuracy of other related techniques is 90% for CNN, 88.34% for AlexNet, 92.01% for ResNet18, and 85.34% for LSTM. Similarly, the precision and recall rate of these existing techniques is lower than that of other techniques. The comparison of F1-score, Specificity, and Kappa are analyzed and represented in Figure 5.

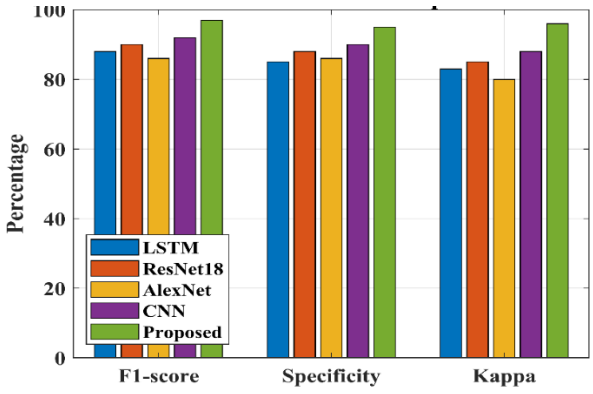

Figure 5: Comparison of F1-score, Specificity and Kappa

The F1-score, Specificity, and Kappa are analyzed using various existing techniques to determine how well the proposed approach performs. By examining the accuracy, Figure 5 illustrates how the suggested strategy outperforms other relevant strategies. The proposed approach yields 97% F1-score, 95% Specificity, and 96% Kappa. By accomplishing these goals, the proposed approach offers effective brain tumor segmentation and prediction. The F1-score of the proposed technique achieves efficient performance compared to LSTM (88%), ResNet18 (90%), AlexNet (86%), and CNN (92%). Similarly, the Specificity and Kappa rate

Received: July 18, 2025

International Journal of Applied Mathematics

Volume 38 No. 3s, 2025

ISSN: 1311-1728 (printed version); ISSN: 1314-8060 (on-line version)

of the suggested technique is higher than other related current methods. Figure 6 denotes accuracy as well as loss rate of training as well as testing.

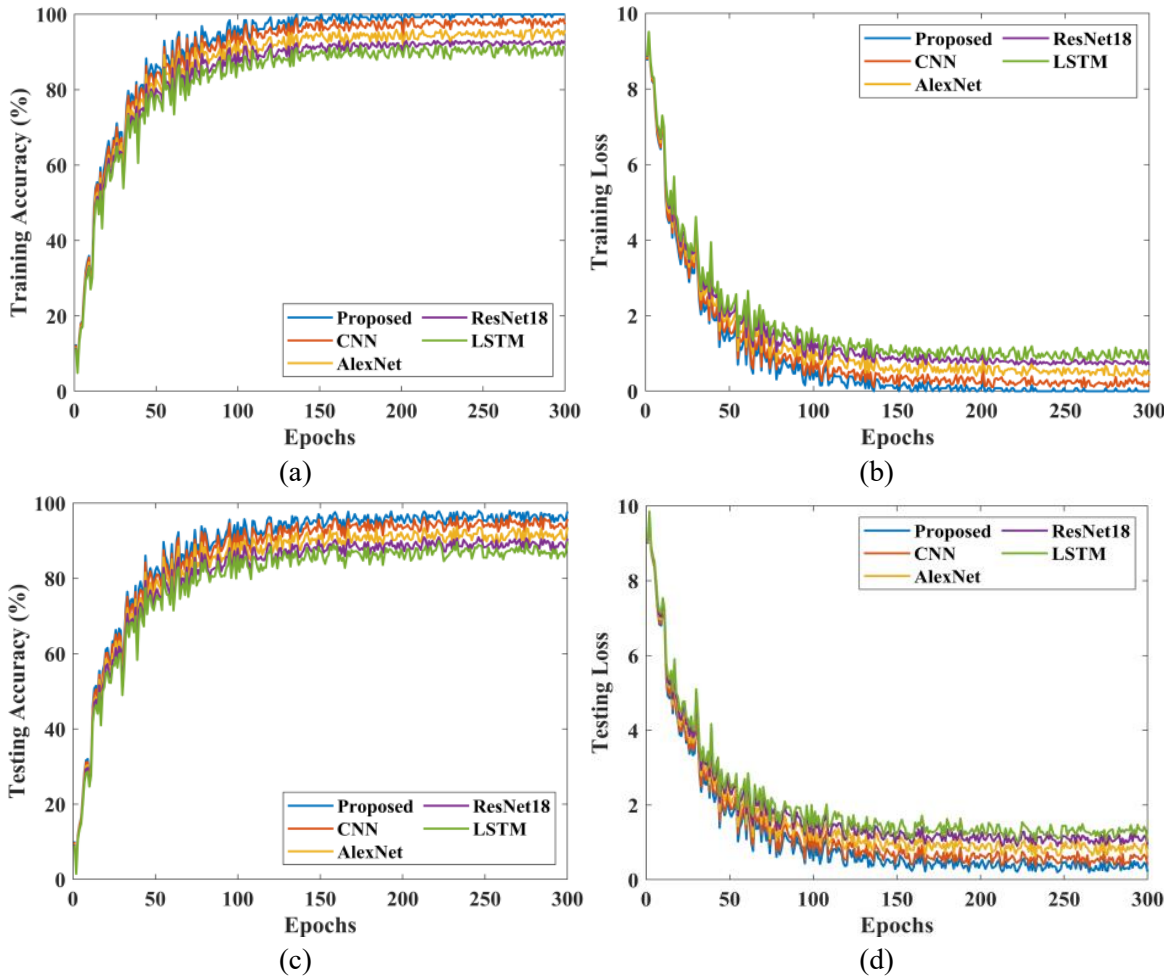

Figure 6: Performance of (a) Training Accuracy, (b) Training Loss, (c) Testing Accuracy and (d) Testing Loss

The accuracy, as well as loss rates of the performance, are analyzed for both training and testing to detect the brain tumor effectively. In this work, the data is split into a 70:30 ratio for training as well as testing. It describes that 70% of data from the dataset are utilized for training the model, and the remaining 30% is utilized for testing. The entire effectiveness of the suggested technique will be assessed, and its superiority will be established based on this training and testing process. When compared to other related procedures, Figures 6(a) and (b) clearly show that the accuracy of both training and testing marginally improves its performance. In the same way, the suggested technique's loss is minimized during testing and training, indicating its effectiveness. The comparison of the MAE, MSE, and RMSE analyses is shown in Figure 7.

Received: July 18, 2025

International Journal of Applied Mathematics

Volume 38 No. 3s, 2025

ISSN: 1311-1728 (printed version); ISSN: 1314-8060 (on-line version)

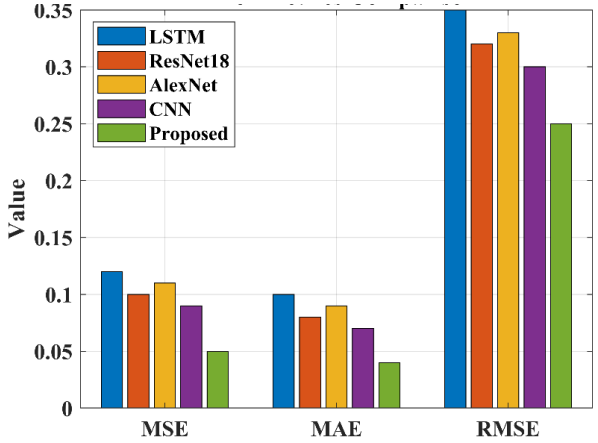

Figure 7: Comparison of MSE, MAE and RMSE

The performance of error metrics, such as MSE, MAE, and RMSE, was analyzed using various related techniques to determine the efficient performance of the suggested method. The error rate of the suggested technique was analyzed using related techniques, including LSTM, ResNet18, AlexNet, and CNN. The proposed technique achieves 0.05 MSE, 0.04 MAE, and 0.25 RMSE, which are lower than those of other related techniques. Figure 7 clearly describes the efficiency of the suggested approach compared to other related techniques. The comparison of the ROC curve is represented in Figure 8.

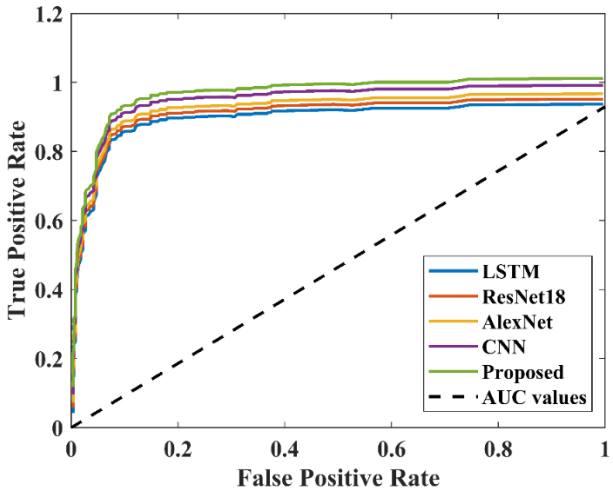

Figure 8: Comparison of ROC curve

The Receiver operating characteristic (ROC) curve of the proposed technique is analyzed based on the AUC value, which is evaluated based on the Area under the ROC curve (AUC) rate. Then, the comparison is conducted to evaluate the efficiency of the suggested technique with other related techniques such as LSTM, ResNet18, AlexNet, and CNN. Figure 8 clearly describes the superiority of the suggested approach as well as other related approaches by comparing the AUC value. The confusion matrix of the suggested technique is represented in Figure 9.

Received: July 18, 2025

International Journal of Applied Mathematics

Volume 38 No. 3s, 2025

ISSN: 1311-1728 (printed version); ISSN: 1314-8060 (on-line version)

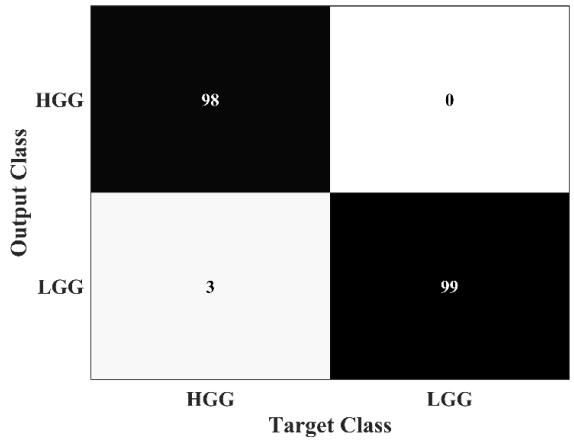

Figure 9: Confusion matrix of the suggested technique

The confusion matrix of the proposed technique was analyzed based on two classes, HGG and LGG. It is mainly utilized to determine the efficient performance of the proposed technique for both classes. In the HGG class, 98 data are correctly classified from 101 data, which achieves efficient prediction. Similarly, the 99 data are correctly classified out of 99 data in the LGG class. It nearly achieves 98% accuracy in classifying the data as HGG and LGG. The computational time of the suggested approach with other related approaches is represented in Figure 10.

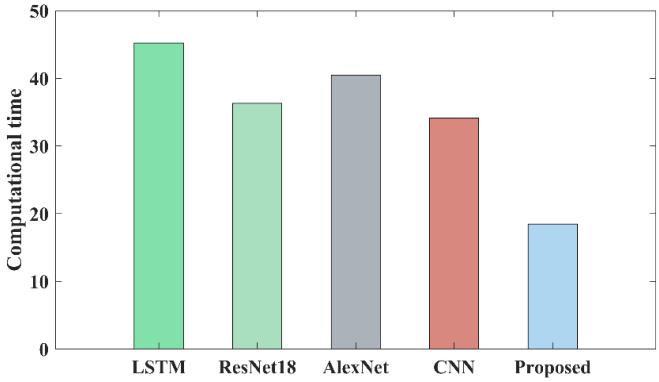

Figure 10: Comparison of computational time

The computational time analyzes the time required for an approach to accurately detect the tumor, which is used to evaluate the proposed technique. Then, the comparison is conducted using various related techniques to determine its efficient performance. The proposed technique requires 18.45 seconds for both brain tumor segmentation and organization. It is lower than other related techniques, such as 45.20 seconds for LSTM, 36.30 seconds for ResNet18, 40.50 seconds for AlexNet, and 34.15 seconds for CNN. It clearly describes the efficient performance of the suggested technique compared to other related approaches.

Received: July 18, 2025

International Journal of Applied Mathematics

Volume 38 No. 3s, 2025

ISSN: 1311-1728 (printed version); ISSN: 1314-8060 (on-line version)

4.4 Discussion

The performance of the proposed technique is analyzed using various related techniques to describe its efficiency. A comparative analysis of the suggested technique with some related approach based on its accuracy is represented in Table 5.

Table 5: Comparative analysis

Author name and reference	Technique use	Dataset used	Accuracy
M.O. Khairandish et al. [28]	Hybrid CNN-SVM	BRATS 2015 dataset	97.43%
Ilyasse Aboussaleh et al. [29]	CNN	BraTS 2017 dataset	91%
Nagwan Abdel Samee et al. [30]	DCNN	BRATS 2015 dataset	88.6%
R. Pitchai et al. [31]	ANN-Fuzzy K means algorithm	BRATS dataset	94%
Angona Biswas and Md. Saiful Islam, [32]	ANN	Figshare dataset	95.4%
Amran Hossain et al. [33]	BINet model	Real-time dataset	High computational complexity
R. Poonguzhali et al. [34]	TSO-GRU model	FigShare dataset	High time consumption
Hanene Sahli et al. [55]	Combined ResNet-SVM model	MRI dataset	89.36% accuracy
proposed	**FT-HDC^{2}Net**	**BraTS 18 dataset**	**98%**

M.O. Khairandish et al. [28] developed a Hybrid CNN-SVM for the BRATS 2015 dataset, which achieves 97.43% accuracy. Ilyasse Aboussaleh et al. [29] presented a CNN model for brain tumor segmentation and classification. This model utilizes the BraTS 2017 dataset, as well as it achieves 91% accuracy. Nagwan Abdel Samee et al. [30] developed DCNN for the BRATS 2015 dataset, which achieves 88.6% of the dataset. Similarly, other related techniques also analyzed its performance with various related techniques to determine its efficiency.

5. Conclusion

The proposed approach is designed to address issues of computational complexity and low performance while providing effective tumor identification. The T1, T2, as well as Flair forms

Received: July 18, 2025

Volume 38 No. 3s, 2025

ISSN: 1311-1728 (printed version); ISSN: 1314-8060 (on-line version)

of MRI images are first extracted from the dataset and pre-processed with image scaling, HSV color channel conversion, and Up-MFil. Next, segmentation based on WT, TC, and ET was carried out using the GKT. In order to minimize dimensionality concerns, the GO_ENetB3 model is used for feature extraction and optimal feature selection. Ultimately, the tumor was classified as an HGG or an LGG using the FT-HDC2Net approach. The WSO algorithm is then applied to adjust the hyperparameter. The suggested approach achieves 98% accuracy, 96% precision, 94% recall, 97% F1-score, 95% Specificity and 96% Kappa. The suggested approach also obtained a low error rate of 0.05 for MSE, 0.04 for MAE, and 0.25 for RMSE. The computation time of the suggested technique is 18.45 seconds. It clearly describes the superiority of the suggested technique for brain tumor segmentation and detection. In the future, the performance of the proposed technique will be improved using advanced DL techniques. Also, a hybrid dataset will be explored to provide efficient classification.

Compliance with Ethical Standards

Funding: No funding is provided for the preparation of the manuscript.

Conflict of Interest: Authors declare that they have no conflict of interest.

Ethical Approval: This article does not contain any studies with human participants or animals performed by any of the authors.

Consent to participate: All the authors involved have agreed to participate in this submitted article.

Consent to Publish: All the authors involved in this manuscript give full consent for publication of this submitted article.

Authors Contributions: All authors read and approved the final manuscript.

Data Availability Statement: Data sharing is not applicable to this article.

References

[1] Sharma P, Shukla AP (2021) A review on brain tumor segmentation and classification for MRI images. In 2021 International Conference on Advance Computing and Innovative Technologies in Engineering (ICACITE) 963-967. IEEE.

[2] Díaz-Pernas FJ, Martínez-Zarzuela M, Antón-Rodríguez M, González-Ortega D (2021) A deep learning approach for brain tumor classification and segmentation using a multiscale convolutional neural network. In Healthcare 9(2): 153. MDPI.

[3] Gull S, Akbar S, Hassan SA, Rehman A, Sadad T (2021) Automated brain tumor segmentation and classification through MRI images. InInternational Conference on Emerging Technology Trends in Internet of Things and Computing 182-194. Cham: Springer International Publishing.

[4] Tataei Sarshar N, Ranjbarzadeh R, Jafarzadeh Ghoushchi S, de Oliveira GG, Anari S, Parhizkar M, Bendechache M (2021) Glioma brain tumor segmentation in four MRI

Received: July 18, 2025

Volume 38 No. 3s, 2025
ISSN: 1311-1728 (printed version); ISSN: 1314-8060 (on-line version)

modalities using a convolutional neural network and based on a transfer learning method. In Brazilian Technology Symposium 386-402. Cham: Springer International Publishing.
[5] Karayegen G, Aksahin MF (2021) Brain tumor prediction on MR images with semantic segmentation by using deep learning network and 3D imaging of tumor region. Biomedical Signal Processing and Control 66:102458.
[6] Sasank VV, Venkateswarlu S (2021) Brain tumor classification using modified kernel based softplus extreme learning machine. Multimedia Tools and Applications 80(9):13513-34.
[7] Ahuja S, Panigrahi BK, Gandhi TK (2021) Fully automatic brain tumor segmentation using DeepLabv3+ with variable loss functions. In 2021 8th International Conference on Signal Processing and Integrated Networks (SPIN) 522-526. IEEE.
[8] Zhang D, Huang G, Zhang Q, Han J, Han J, Yu Y (2021) Cross-modality deep feature learning for brain tumor segmentation. Pattern Recognition 110:107562.
[9] Arora S, Sharma M (2021) Deep learning for brain tumor classification from mri images. In 2021 Sixth International Conference on Image Information Processing (ICIIP) 6: 409-412. IEEE.
[10] Maas B, Zabeh E, Arabshahi S (2021) QuickTumorNet: fast automatic multi-class segmentation of brain tumors. In 2021 10th international IEEE/EMBS conference on neural engineering (NER) 81-85. IEEE.
[11] Aamir M, Rahman Z, Dayo ZA, Abro WA, Uddin MI, Khan I, Imran AS, Ali Z, Ishfaq M, Guan Y, Hu Z (2022) A deep learning approach for brain tumor classification using MRI images. Computers and Electrical Engineering 101:108105.
[12] Zhang W, Wu Y, Yang B, Hu S, Wu L, Dhelim S (2021) Overview of multi-modal brain tumor mr image segmentation. InHealthcare 9(8): 1051. MDPI.
[13] Budati AK, Katta RB (2022) An automated brain tumor detection and classification from MRI images using machine learning technique s with IoT. Environment, Development and Sustainability 24(9):10570-84.
[14] Rehman A, Khan MA, Saba T, Mehmood Z, Tariq U, Ayesha N (2021) Microscopic brain tumor detection and classification using 3D CNN and feature selection architecture. Microscopy Research and Technique 84(1):133-49.
[15] Ranjbarzadeh R, Zarbakhsh P, Caputo A, Tirkolaee EB, Bendechache M (2024) Brain tumor segmentation based on optimized convolutional neural network and improved chimp optimization algorithm. Computers in Biology and Medicine 168:107723.
[16] Garg G, Garg R (2021) Brain tumor detection and classification based on hybrid ensemble classifier. arXiv preprint arXiv:2101.00216.
[17] Shoaib MR, Elshamy MR, Taha TE, El-Fishawy AS, Abd El-Samie FE (2022) Efficient deep learning models for brain tumor detection with segmentation and data augmentation techniques. Concurrency and Computation: Practice and Experience 34(21):e7031.
[18] Arbane M, Benlamri R, Brik Y, Djerioui M (2021) Transfer learning for automatic brain tumor classification using MRI images. In 2020 2nd international workshop on human-centric smart environments for health and well-being (IHSH) 210-214. IEEE.

Received: July 18, 2025

Volume 38 No. 3s, 2025
ISSN: 1311-1728 (printed version); ISSN: 1314-8060 (on-line version)

[19] Masood M, Nazir T, Nawaz M, Mehmood A, Rashid J, Kwon HY, Mahmood T, Hussain A (2021) A novel deep learning method for recognition and classification of brain tumors from MRI images. Diagnostics 11(5):744.
[20] Vankdothu R, Hameed MA (2022) Brain tumor segmentation of MR images using SVM and fuzzy classifier in machine learning. Measurement: Sensors 24:100440.
[21] Zhang H, Wei Z, Liu G, Wang R, Mu R, Liu C, Yuan A, Cao G, Hu N. MKEAH: Multimodal knowledge extraction and accumulation based on hyperplane embedding for knowledge-based visual question answering. Virtual Reality & Intelligent Hardware. 2024;6(4):280-91.
[22] Li M, Jung Y, Fulham M, Kim J. Importance-aware 3D volume visualization for medical content-based image retrieval-a preliminary study. Virtual Reality & Intelligent Hardware. 2024;6(1):71-81.
[23] Guerroudji MA, Amara K, Lichouri M, Zenati N, Masmoudi M. A 3D visualization-based augmented reality application for brain tumor segmentation. Computer Animation and Virtual Worlds. 2024;35(1):e2223.
[24] Xiao Z, Chen Y, Zhou X, He M, Liu L, Yu F, Jiang M. Human action recognition in immersive virtual reality based on multi-scale spatio-temporal attention network. Computer Animation and Virtual Worlds. 2024 Sep;35(5):e2293.
[25] Nazir A, Cheema MN, Sheng B, Li P, Li H, Xue G, Qin J, Kim J, Feng DD. Ecsu-net: an embedded clustering sliced u-net coupled with fusing strategy for efficient intervertebral disc segmentation and classification. IEEE Transactions on Image Processing. 2021;31:880-93.
[26] Nazir A, Cheema MN, Sheng B, Li H, Li P, Yang P, Jung Y, Qin J, Kim J, Feng DD. OFF-eNET: An optimally fused fully end-to-end network for automatic dense volumetric 3D intracranial blood vessels segmentation. IEEE Transactions on Image Processing. 2020;29:7192-202.
[27] Wei B, Wen Y, Liu X, Qi X, Sheng B. SOFNet: optical-flow based large-scale slice augmentation of brain MRI. Displays. 2023;80:102536.
[28] Khairandish MO, Sharma M, Jain V, Chatterjee JM, Jhanjhi NZ (2022) A hybrid CNN-SVM threshold segmentation approach for tumor detection and classification of MRI brain images. Irbm 43(4):290-9.
[29] Aboussaleh I, Riffi J, Mahraz AM, Tairi H (2021) Brain tumor segmentation based on deep learning's feature representation. Journal of Imaging 7(12):269.
[30] Samee NA, Ahmad T, Mahmoud NF, Atteia G, Abdallah HA, Rizwan A (2022) Clinical decision support framework for segmentation and classification of brain tumor MRIs using a U-Net and DCNN cascaded learning algorithm. In Healthcare 10(12): 2340. MDPI.
[31] Pitchai R, Supraja P, Victoria AH, Madhavi MJ (2021) Brain tumor segmentation using deep learning and fuzzy K-means clustering for magnetic resonance images. Neural Processing Letters 53:2519-32.

Received: July 18, 2025

Volume 38 No. 3s, 2025
ISSN: 1311-1728 (printed version); ISSN: 1314-8060 (on-line version)

[32] Biswas A, Islam MS (2021) Brain tumor types classification using K-means clustering and ANN approach. In 2021 2nd International Conference on Robotics, Electrical and Signal Processing Techniques (ICREST) 654-658. IEEE.

[33] Hossain A, Islam MT, Rahman T, Chowdhury ME, Tahir A, Kiranyaz S, Mat K, Beng GK, Soliman MS. Brain tumor segmentation and classification from sensor-based portable microwave brain imaging system using lightweight deep learning models. Biosensors. 2023 Feb 21;13(3):302.

[34] Poonguzhali R, Ahmad S, Sivasankar PT, Babu SA, Joshi P, Joshi GP, Kim SW. Automated brain tumor diagnosis using deep residual u-net segmentation model. Computers, Materials & Continua. 2023 Jan 1;74(1):2179-94.

[35] Sahli H, Ben Slama A, Zeraii A, Labidi S, Sayadi M. ResNet-SVM: Fusion based glioblastoma tumor segmentation and classification. Journal of X-ray science and technology. 2023 Jan 27;31(1):27-48.

[36] Zhao ML, Ni SQ, Du ZG, Wang XY, Tian AQ, Ma XL (2023) Multi-Objective Gannet Optimization Algorithm for Dynamic Passenger Flow Allocation in Train Operation Plan Optimization. IEEE Access.

[37] Alhichri H, Alswayed AS, Bazi Y, Ammour N, Alajlan NA (2021) Classification of remote sensing images using EfficientNet-B3 CNN model with attention. IEEE access 9:14078-94.

[38] Qin J, Pan W, Xiang X, Tan Y, Hou G (2020) A biological image classification method based on improved CNN. Ecological Informatics 58:101093.

[39] Makhadmeh SN, Al-Betar MA, Assaleh K, Kassaymeh S (2022) A hybrid white shark equilibrium optimizer for power scheduling problem based IoT. IEEE Access 10:132212-31.

Received: July 18, 2025